JCTC Journal of Chemical Theory and Computation

Article

Cite This: J. Chem. Theory Comput. 2019, 15, 2022−2032

pubs.acs.org/JCTC

NanoModeler: A Webserver for Molecular Simulations and Engineering of Nanoparticles

Sebastian Franco-Ulloa, Laura Riccardi, Federico Rimembrana, Mattia Pini, and Marco De Vivo*

Molecular Modeling and Drug Discovery Lab, Istituto Italiano di Tecnologia, via Morego 30, Genova 16163, Italy

ABSTRACT: Functionalized nanoparticles (NPs) are at the frontier of nanoscience. They hold the promise of innovative applications for human health and technology. In this context, molecular dynamics (MD) simulations of NPs are increasingly employed to understand the fundamental structural and dynamical features of NPs. While informative, such simulations demand a laborious two-step process for their setup. In-house scripts are required to (i) construct complex 3D models of the inner metal core and outer layer of organic ligands, and (ii) correctly assign force-field parameters to these composite systems. Here, we present NanoModeler (www.nanomodeler.it), the first Webserver designed to automatically generate and parametrize model systems of monolayer-protected gold NPs and gold nanoclusters. The only required input is a structure file of one or two ligand(s) to be grafted onto the gold core, with the option of specifying homogeneous or heterogeneous NP morphologies. NanoModeler then generates 3D models of the nanosystem and the associated topology files. These files are ready for use with the Gromacs MD engine, and they are compatible with the AMBER family of force fields. We illustrate NanoModeler's capabilities with MD simulations of selected representative NP model systems. NanoModeler is the first platform to automate and standardize the construction and parametrization of realistic models for atomistic simulations of gold NPs and gold nanoclusters.

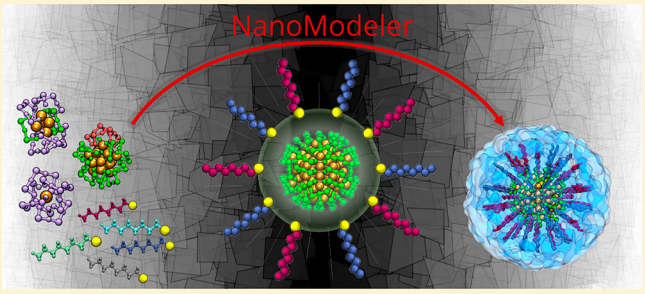

INTRODUCTION

Monolayer-protected metal nanoparticles (NPs) are nanosized molecules comprising a metallic inner core covered by an organic layer with a varying number of coating ligands. These ligands shield the NP core and dictate the supramolecular chemistry at the NP surface. They can be functionalized in different ways, generating NPs with diverse structural and chemico-physical properties. For example, functionalized NPs can recognize selected substrates with programed specificity and affinity,[1] and can catalyze chemical transformations (i.e., nanozymes).[2−4] Functionalized NPs have thus found application in bioimaging,[5] photothermal therapy,[6−8] drug delivery,[9−11] and other fields.[12−15]

Because of their flexible chemical structure, it is difficult to examine the organization and dynamics of the coating ligands in functionalized NPs. However, understanding the fundamental dynamical behavior of the coating ligands is necessary to rationally design functionalized NPs with programmed abilities.[1,16] In this context, atomistic molecular dynamics (MD) simulations can significantly improve our understanding of the ligand dynamics and interactions at the basis of NP applications, including NMR-based chemosensing[1,17] and nanocatalysis.[3,18] For example, MD simulations take full account of the molecule's flexibility in explicit solvents.[19,20] They are thus suitable for elucidating NP dynamics and flexibility.[21] As a result, the literature contains a growing number of studies that combine MD simulations with experiments to investigate NPs involved in complex phenomena, including penetration of lipid bilayers,[22−28] protein/lipid corona formation,[29−31] and particle aggregation.[32,33]

It is not easy to construct realistic 3D models of NPs and their parametrization for MD simulations.[34] There are many tools for building and parametrizing macromolecules such as proteins,[35−38] nucleic acids,[39−41] and lipids.[42−44] However, there are no standardized tools for building and parametrizing complex NP models for MD simulations. Computational researchers must develop in-house software to build such models, and prepare ad hoc protocols to create the NP topology, which includes all of the force-field parameters for MD simulations (e.g., bonded and nonbonded parameters). This process can be quite complex, and it is certainly laborious.

Here, we present NanoModeler (www.nanomodeler.it), the first Webserver for the automatic and standardized construction and parametrization of realistic models for use in atomistic MD simulations of gold NPs (AuNPs) and nanoclusters. This tool facilitates the investigation and engineering of AuNPs and nanoclusters, onto which molecular composites can be grafted to form a functionalized monolayer.

Many AuNPs and nanocluster structures have become available in experimental and theoretical studies,[45−48] with NPs used as biosensors[49,50] and contrast agents.[51,52] This growing body of experimental data has prompted the parametrization of these NPs for MD simulations. On the basis of these data, NanoModeler generates 3D models and topologies for

Received: December 28, 2018
Published: February 13, 2019

DOI: 10.1021/acs.jctc.8b01304
J. Chem. Theory Comput. 2019, 15, 2022−2032

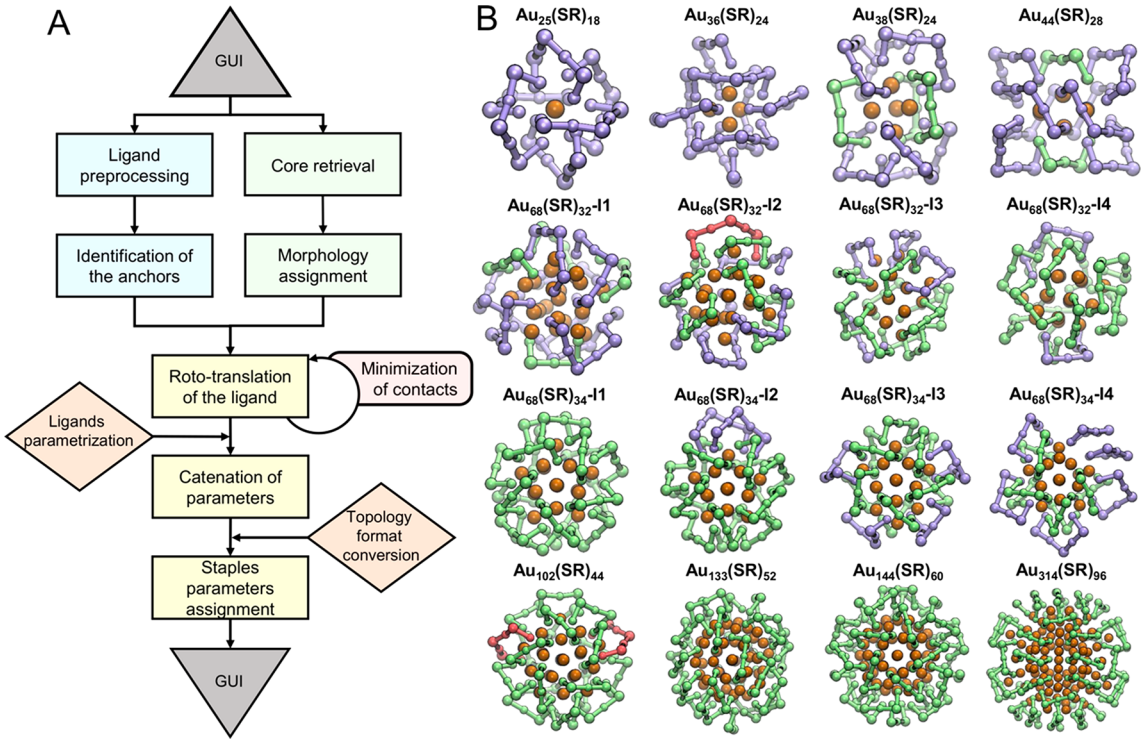

Figure 1. (A) Workflow of NanoModeler upon job submission. The graphical user interface is in gray. Steps involving only the ligand are in blue; those involving the core are in green; those involving both the core and the ligands are in yellow. External software dependencies are in orange, and additional steps are in red. (B) Entire core structure of the available cores that can be used to build functionalized nanoparticles. In each core supported by NanoModeler, staples, the anchoring sites to which the coating ligands are coupled, are displayed in green, purple, and red. In more detail, staples of type STR are in green, STC in purple, and STV in red. For a detailed definition of the staple types (STR, STC, and STV), as well as of their associated atom types, please refer to Figure 2.

Table 1. List of the 16 Cores Supported by NanoModeler, Identified by Their Gold-to-Sulfur Ratio[a]

core	size (nm)	STR	STC	STV	original ligand	remarks
$Au_{25}(SR)_{18}$	0.9		6		phenylethanethiol	ref 104
$Au_{36}(SR)_{24}$	1.1		8		cyclopentanethiol	ref 105
$Au_{38}(SR)_{24}$	1.1	3	6		phenylethanethiol	ref 106
$Au_{44}(SR)_{28}$	1.1	2	8		methanethiol	ref 107
$Au_{68}(SR)_{32}$	1.3	4	8		none	isoform 1, ref 108
$Au_{68}(SR)_{32}$	1.3	7	5	1	none	isoform 2, ref 108
$Au_{68}(SR)_{32}$	1.3	10	4		none	isoform 3, ref 108
$Au_{68}(SR)_{32}$	1.3	13	2		none	isoform 4, ref 108
$Au_{68}(SR)_{34}$	1.2	17			none	isoform 1, ref 109
$Au_{68}(SR)_{34}$	1.3	14	2		none	isoform 2, ref 109
$Au_{68}(SR)_{34}$	1.3	11	4		none	isoform 3, ref 109
$Au_{68}(SR)_{34}$	1.4	8	6		none	isoform 4, ref 109
$Au_{102}(SR)_{44}$	1.5	19		2	*p*-mercaptobenzoic acid	ref 110
$Au_{133}(SR)_{52}$	1.7	26			*p*-*tert*-butylbenzenethiol	ref 111
$Au_{144}(SR)_{60}$	1.7	30			*p*-mercaptobenzoic acid	ref 112
$Au_{314}(SR)_{96}$	2.1	48			none	ref 48

[a]The table also reports the average diameter as well as the number and type of staples present on each core. Staples are the anchoring sites to which the coating ligands are coupled, and are here named as STR, STC, and STV on the basis of their chemical structure and atomic connectivity. For a detailed definition of staple types, as classified in NanoModeler, please refer to Figure 2. The ligand with which the system was originally elucidated (if present) and the respective reference are also shown.

homogeneous and mixed monolayer-protected AuNPs. These models are ready to be investigated via MD simulations. One or two ligand types can be considered when building a 3D model of the NPs, which are then assembled to produce a topology file that is compatible with the AMBER family of force fields.

In summary, NanoModeler allows the automatic setup of atomistic MD simulations of multifaceted mixtures of functionalized NPs. This novel tool will help researchers study and engineer functionalized gold NPs and nanoclusters, while serving as a technological platform for future software developments related to MD simulations of NPs.

DOI: 10.1021/acs.jctc.8b01304
J. Chem. Theory Comput. 2019, 15, 2022−2032

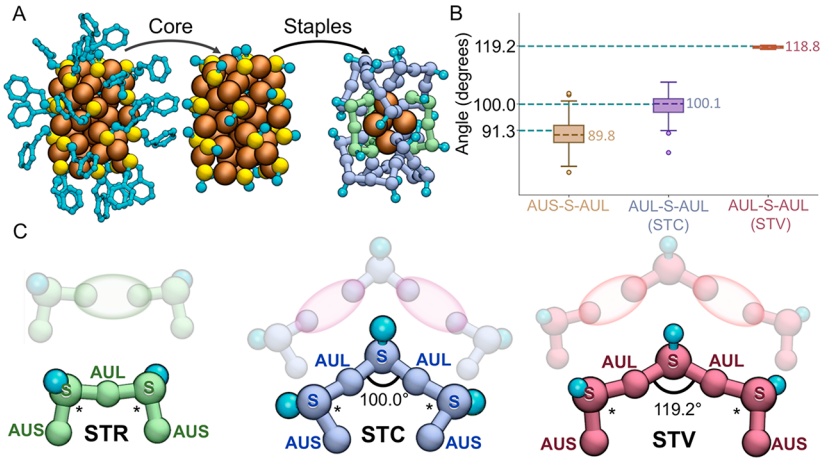

Figure 2. (A) X-ray-derived structure for $Au_{38}(PET)_{24}$, its core as incorporated in NanoModeler, and the staple-type classification. Gold atoms are in brown, sulfur in yellow, and carbon in cyan. (B) Boxplot for the different types of gold−sulfur−gold angles in the staples, in all 16 cores. The colored numbers represent the median of each distribution, whereas the aquamarine lines indicate the equilibrium values as derived by Pohjolainen and co-workers.[72] (C) The three staple types considered in NanoModeler are shown. Staples are the anchoring sites used to couple the coating ligands to the core of the nanoparticle. The staple named STR comprises two intersecting subunits, while staples named STC and STV comprise three subunits. Each subunit includes one sulfur atom, plus the nearest two gold atoms and one carbon atom. Subunits are shown in transparency on top of each staple. AUL and AUS are atom types used in NanoModeler to classify gold atoms that belong to staples. AUL or AUS indicate their specific position in the respective staple. The atom type S indicates sulfur atoms. Notably, STC and STV differ only in the AUL−S−AUL angle. The AUS−S−AUL angles are indicated with a star (*). STR residues are in green, STC in purple, and STV in red.

RESULTS AND DISCUSSION

The NanoModeler Webserver (www.nanomodeler.it) is a free service, which the scientific community can use to prepare the necessary files for MD simulations of monolayer-protected AuNPs and gold nanoclusters. The backend of the tool is coded in Python. The frontend uses a mixture of HTML, CSS, and JavaScript. The NanoModeler Website includes documentation and tutorials, which describe the overall process for setting up the system of interest, and the available options. Below, we explain how NanoModeler operates, step by step, as per the workflow in Figure 1A.

Building a 3D Model of AuNPs. When using MD simulations to obtain an atomistic understanding of AuNPs, the user must build a reliable 3D model of the NP of interest. The structure of AuNPs can be divided into three characteristic building blocks: (i) the inner quasi-static gold atoms; (ii) the gold−sulfur staple-like motifs positioned on the surface of the core; and (iii) the coating ligands linked to the staple-like motifs. NanoModeler uses these three building blocks to construct and assemble the final AuNP model.

Importantly, the key properties and interaction patterns of AuNPs also depend on the size of the metal core.[53,54] In recent years, experimental and theoretical studies have elucidated several structures of AuNPs and nanoclusters. The cores from these studies are incorporated into NanoModeler (Table 1). NanoModeler offers 16 different cores ranging in diameter from 0.9 ($Au_{25}(SR)_{18}$) to 2.1 nm ($Au_{314}(SR)_{96}$, Figure 1B). Each core structure can be used as the supporting body to assemble the final AuNP. We define the core as the coordinates of the gold atoms and the 3D disposition of the sulfur atoms, including the first carbon of the ligands, as originally placed in the template AuNP structure (Figure 2A).

Each specific core also defines the structure and disposition of the gold−sulfur interface "staples",[55,56] some of which are depicted in Figure 2. These motifs act as anchoring sites, to which the coating ligands are coupled. NanoModeler supports three staple types, hereafter named STR, STC, and STV, with differing connectivity and angle parameters (Figure 2). Each one includes two or three sulfur atoms. In all three staple types, each sulfur atom is bound to two gold atoms and one carbon atom. Notably, certain cores exist in different isoforms, that is, as the same core with a different number of staples organized in distinctive arrangements. For example, the $Au_{68}(SR)_{32}$ and $Au_{68}(SR)_{34}$ cores in NanoModeler result in four isoforms of comparable dimensions, which differ in the type and location of the staples.

The staples of a given core have a static arrangement that, in turn, fixes the total amount of ligands to be placed on each of the cores. Moreover, due to the chiral nature of the ligand's sulfur atoms, the ligands can be located on different sides with respect to the staples' plane, leading to cis−trans isomers.[55,57,58] The number of isomers depends on the size and specific number of staples, and can quickly become unmanageably high. For example, the 1.1 nm $Au_{38}(SR)_{24}$ nanocluster already admits 2^{24} cis−trans stereoisomers.[59] Even in the smallest systems, the number of isomers is unmanageable. As a result, NanoModeler allows the user to treat cis−trans isomerism in two ways. First, NanoModeler can keep the isomerism with which the core was originally elucidated. Second, the first carbon atom of each ligand can be placed along the vector formed between the system's centroid and the sulfur atoms. The latter method produces an out-of-equilibrium structure, which attempts to be equidistant from all possible isomers.

In addition to all of the possible sizes, staple distributions, and cis−trans isomers considered in NanoModeler, AuNPs allow the user to implement thiols with great chemical diversity. The thiols' chemical structure (as a .mol2 file) is the only input required by NanoModeler. In this way, AuNPs and nanoclusters can be coated by functionalized thiols, with the structure specified by the user. These thiols can also be placed to form homogeneous or mixed monolayers. For homogeneous monolayers, a unique ligand uniformly covers the metallic core's surface. For heterogeneous monolayers, two

DOI: 10.1021/acs.jctc.8b01304
J. Chem. Theory Comput. 2019, 15, 2022−2032

coating ligands can be arranged in different ways over the NP's surface to give rise to various morphologies.[60] These morphologies include random,[61,62] Janus-like,[63,64] and striped[17,65−67] distributions, all of which are accessible by NanoModeler (Figure 3). These distributions are a key factor in the overall behavior of AuNPs.[17,68−71]

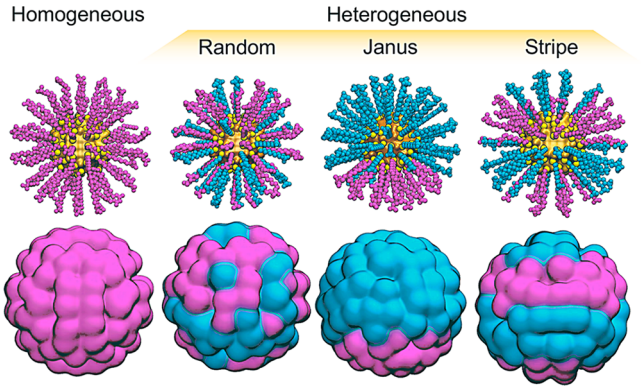

Figure 3. Graphical representation of the four morphologies supported by NanoModeler. If only one coating ligand is provided, the outcome is a homogeneous monolayer-protected AuNP (first column). If two coating ligands (pink and cyan) are provided, the other three morphologies become available. These morphologies correspond to random, Janus-like, and striped distributions, displayed in the second, third, and fourth columns, respectively. Gold atoms are shown in brown, sulfur atoms in yellow, and two arbitrary ligands in pink and cyan.

Thus, NanoModeler can assemble monolayer-protected AuNPs, each defined by a given size, geometry, 3D shape, and functionalization. It can output these AuNPs in common file formats (.pdb and .gro). The building and assembly operations can implement a variety of different cores, from subnanometer-sized nanoclusters up to 2 nm AuNPs. The available cores also consider diverse staple arrangements, accounting for possible conformers. Furthermore, NanoModeler allows the assembly of both homogeneous and heterogeneous monolayers, with random, Janus-like, or striped distributions of the grafted thiols.

Building Topologies for MD Simulations of AuNPs. To run MD simulations, each AuNP's 3D model requires bonded and nonbonded parameters, such as force constants, equilibrium values, atomic partial charges, and Lennard-Jones coefficients. These are eventually used to build the topology of a given AuNP, which is used to compute the forces and evolve the system according to Newton's equations of motion in MD simulations. Over the years, several groups have developed parameters for simulating selected functionalized gold cores.[72−74] Here, after collecting all of the available parameters, we have automatized the creation of topology files for each given AuNP of interest. In NanoModeler, the parameter file is written in a Gromacs-compatible format (.top).

NanoModeler builds the topology file in a way similar to building the 3D model, from the inside to the outside of the structure. Starting from the inner metallic core, NanoModeler uses the nonbonded parameters of gold generated by Heinz and co-workers.[73] For this implementation, gold atoms are categorized as AUL or AUS if they belong to staples (see more below on parameters for staples). AUL or AUS differ in their specific position in the respective staple (Figure 2). All of the remaining gold atoms of the system are assigned the AU atom type. Notably, AU atom types are not subject to any bonding forces. Instead, they are only treated using the van der Waals term.[72] All of the gold atoms in a given AuNP are assigned a charge of zero. Considering charged gold atoms does not increase the accuracy of MD simulations because the electrostatic potential quickly goes to zero on the core's surface.[24,72,74]

NanoModeler implements bonded and nonbonded parameters for the staple motifs, which are taken from Pohjolainen et

Table 2. Compilation of All of the Nonbonded and Bonded Parameters Implemented in NanoModeler[a]

Bond	k_b (kJ mol^{-1} nm^{-2})	x_0 (nm)
AUS – S	62730.0	0.241
AUL – S	62730.0	0.233
CA – S	198321.6	0.175
CT – S	99113.0	0.184
Angle	**k_θ (kJ mol^{-1} rad^{-2})**	**θ_0 (degrees)**
AUS – S – AUL	460.24	91.3
S – AUL – S	460.24	172.4
AUL – S – AUL (STC)	460.24	100.0
AUL – S – AUL (STV)	1460.24	119.2
AUS – S – C*	146.37	111.6
AUL – S – C*	146.37	106.8
CA – C – OH	585.76	112.0
CA – C – O	585.76	126.0
CA – CA – S	418.40	120.0
S – CT – HC	418.40	107.0
H1 – CT – CA	418.40	109.0
Dihedral	**k_ψ (kJ mol^{-1})**	**ψ_0 (degrees)**
X – X – CA – S	4.6024	180.0
C – CA – CA – CA	4.6024	180.0
Nonbonded	**σ (nm)**	**ε (kJ mol^{-1})**
AU / AUL / AUS	0.2629	22.133
S	0.3563	1.046

[a]Nonbonded parameters are adapted from Heinz et al.,[73] whereas the bonded parameters are taken from Pohjolainen et al.[72]

DOI: 10.1021/acs.jctc.8b01304
J. Chem. Theory Comput. 2019, 15, 2022−2032

al.[72] (Table 2). The classification of staples used in ref 72 to derive the bonded parameters is also appropriate for the extended data set implemented in our Webserver. Thus, NanoModeler classifies the type of staples (i.e., STR, STC, STV, Figure 2C) on any given core, and assigns the corresponding bonded parameters from ref 72. To this end, NanoModeler first divides the staples into subunits comprising one sulfur atom, one carbon atom, and two gold atoms. In total, NanoModeler stores as many subunits as sulfur atoms in the core. Thus, each subunit includes one sulfur atom, plus the nearest two gold atoms and one carbon atom. The staple is then classified as STR, STC, or STV, on the basis of the number of consecutive intersecting subunits and the AUL−S−AUL angle formed in the central subunit. It is important to note that there are two nonoverlapping distributions for the AUL−S−AUL angle (i.e., STC distribution does not overlap with STV distribution in the plot in Figure 2B). Indeed, these distributions correspond to the two different staple types STC and STV, which have an average AUL−S−AUL angle of 100.0° and 119.2°, respectively. Notably, in Figure 2B, the distribution on the angles associated to the STV staple is narrower than that for STC and for the AUS−S−AUL angle. However, this may be due to a varying number of samples for the three sets used to calculate the distribution for each of the angles in the staples. In detail, the AUS−S−AUL angle is present 548 times among the implemented cores and the AUL−S−AUL (STC) angle is present 59 times, while the AUL−S−AUL (STV) angle is present only 3 times in our data set (Table 1). Thus, the narrower distribution of the AUL−S−AUL (STV) angle is due to the limited number of values for the AUL−S−AUL (STV) angle reported in the literature for the considered cores. Once the staple type is identified, the respective bonded parameters are assigned for each subunit (Table 2).[72,73] Finally, NanoModeler assigns parameters to the functionalized coating thiols. Partial atomic charges of the thiol must be present in the input.mol2 file. The server assigns the bonded and Lennard-Jones parameters, calculated with the "parmchk2" tool in AmberTools18,[35,36] and derived from the GAFF force field.[75] In this way, a unique topology file is generated, and then the *acpype.py* script[76] is used to convert the topology file to a Gromacs-compatible format. The user also has the option of uploading a parameters file to overwrite or complete those provided by default.

As output, NanoModeler provides the structure of the input ligands (.mol2 file format), the structure of the assembled AuNP (.pdb and .gro file format), and the parameters of the functionalized NP (.top file format). The structure (.gro) and topology (.top) files are ready to use with the Gromacs MD engine. NanoModeler currently supports 16 cores containing up to three different staple types (STR, STC, and STV), and with specified coating ligands arranged in four possible morphologies (homogeneous, random, Janus, striped). The resulting topology files are ready for use in atomistic MD simulations. All parameters are compatible with the AMBER family of force fields, so the parametrized AuNPs can be simulated in complex mixtures containing biologically relevant macromolecules, such as proteins,[77,78] nucleic acids,[79−83] lipids,[84−86] and carbohydrates.[87]

MD Simulations and Test Cases. To demonstrate NanoModeler's capabilities and potential for studying and engineering AuNPs and nanoclusters, we built three different model systems and validated them by performing 200 ns-long MD simulations, comparing different observables to experimental data. The first system (NP1) was based on the $Au_{314}(SR)_{96}$ core, coated with a homogeneous monolayer of octanethiol. The second system (NP2) was based on the $Au_{144}(SR)_{60}$ core, passivated with decanethiol. The third system (NP3) was based on the $Au_{314}(SR)_{96}$ core, covered with dodecanethiol. We used NanoModeler to generate the topology of each model system. Each model was simulated in a different organic solvent, as used in the experiments (see Webserver Building for details).

Considering that the simulated systems differ in the chemical structure of the coating thiols as well as in the core size and the surrounding solvent, we first verified the stability of the metallic cores. For this, we calculated the RMSD of the staples in NP1, NP2, and NP3, as well as the RMSD of the atoms with type AU (i.e., inner core atoms). As it can be seen from Figure 4A, the staples present and AU atoms are highly stable, with deviations smaller than 0.1 nm as compared to the starting model, in all of the simulated nanoparticles. The low RMSD of the AU atoms alone (~0.013 nm) verifies that the exclusive-van der Waals term suffices to restrain the shape of the metallic substructure.[72]

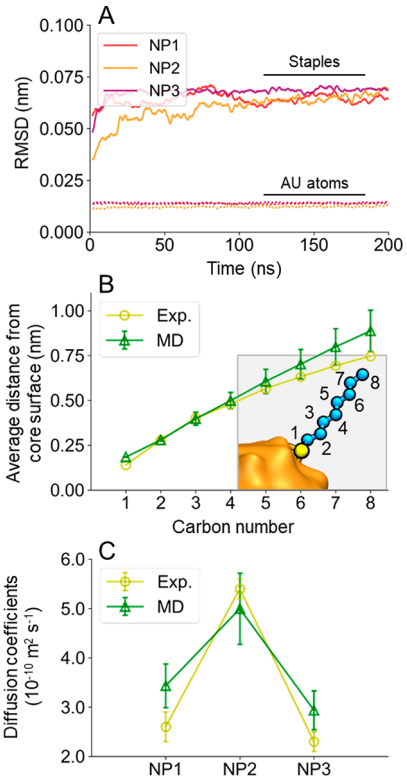

Figure 4. (A) Moving averages calculated from the root-mean-square deviations of the staples and the AU atom types for NP1, NP2, and NP3. The moving averages were calculated with a window size of 20 frames (i.e., 200 ps). (B) The average distance between the metallic core and the carbon atoms of the alkyl chains coating NP1. The average distances from the core's surface is computed as expectation values (and their associated standard deviation) from the radial distribution function of the carbon atoms as explained in detail in the Webserver Building section. The values calculated from our MD simulations are shown in green, whereas the experimental values are in yellow. (C) Calculated and experimental values for the translational diffusion coefficients of the three systems under study. The diffusion coefficients of NP1 and NP3 were measured in chloroform, while the diffusion coefficient for NP2 was measured in dichloromethane.

DOI: 10.1021/acs.jctc.8b01304
J. Chem. Theory Comput. 2019, 15, 2022−2032

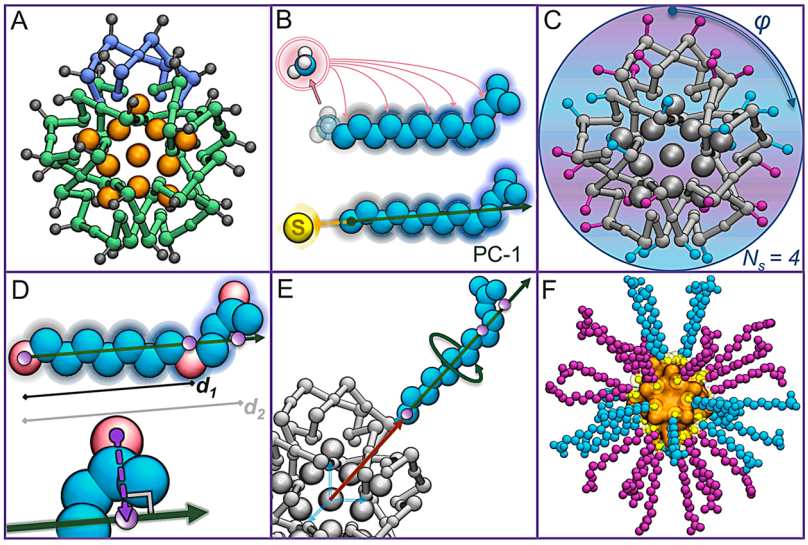

Figure 5. Graphical description of how NanoModeler operates. (A) Generic structure of a core. (B) Initial treatment of coating ligands. The charge of an eventual capping group is distributed across the other atoms in the ligand. If *S* is absent, NanoModeler places it along the compound's first principal component (PC-1). (C) Assignment of a morphology and, in particular, the assignment of a striped distribution of the thiols. (D) Determination of d_1 and d_2 as the distances between *C* and the projection along PC-1 of two randomly chosen atoms. (E) Roto-translation of one ligand into its respective site. (F) Final model obtained for an AuNP with a striped conformation. Inner gold atoms are shown in brown, STR staples in green, STC staples in light purple, two arbitrary ligands are in pink and cyan, randomly chosen atoms for the roto-translation of a ligand are in red, and virtual sites are in dark purple.

For NP1, we first calculated the average distance between the core's surface and each carbon atom of the alkyl chains in chloroform. As depicted in Figure 4B, the simulated and experimental[88,89] results are in excellent agreement. Moreover, the linear ascent of the curves indicates that the alkyl chains around the metallic core are extended toward the organic solvent, as was already reported for similar systems.[1] The nearly spherical conformation of NP1 is also supported by its average eccentricity of 0.014 ± 0.001 calculated from our MD simulations.

We then calculated the translational diffusion coefficient for NP1, NP2, and NP3 using the Stokes−Einstein relation (see Webserver Building for details). Here too, the computed coefficients are in qualitative agreement with the experimental values (Figure 4C).[88,90] In the experiments and simulations, the coefficient for NP2 was assessed by dissolving it in dichloromethane, whereas NP1 and NP3 were solvated in chloroform. The elevated diffusion coefficient of NP2 is thus a consequence of the decreased viscosity of dichloromethane with respect to that of chloroform. Moreover, the approach used to calculate the diffusion coefficients has already been applied to similar systems in dichloromethane by Piserchia and co-workers.[90] In line with this work, an overestimation of the hydrodynamic radius leads to an apparent decrease in the diffusion coefficient, as with NP2 in our simulations.

Finally, we further characterized NP3 by estimating its radius of gyration. Our simulations returned a value of 1.160 ± 0.003 nm, which is in reasonable agreement with the experimental value of 0.924 ± 0.005 nm. The discrepancy might be due to the rigidity of the gold−sulfur interface in NP3, and possible dynamic processes such as diffusion and/or exchange of thiolates on the coating monolayer of gold NPs.[55]

Taken together, these test cases demonstrate that NanoModeler can be used for the setup of molecular dynamics simulations to eventually analyze structural dynamics and calculate chemicophysical properties of AuNPs and nanoclusters, leading to a deeper understanding of the solubility, effective radii, diffusion profiles, and NMR spectra.

CONCLUSIONS

In this work, we present NanoModeler, the first web-based platform for building 3D models of gold NPs and nanoclusters and the topology setup needed for atomistic molecular dynamics (MD) simulations. These models are generated from three building blocks: (i) the inner quasi-static gold atoms, (ii) the gold−sulfur interface, and (iii) the coating ligands. The former two building blocks are retrieved from experimental and high-level computational studies (Tables 1 and 2). The third building block must be provided by the user, and allows the construction of specific functionalized thiols for grafting onto the AuNP of interest. Moreover, NanoModeler allows the assembly of NPs with different types of coating thiols, thus forming mixed-monolayer protected AuNPs and nanoclusters. Finally, these models are used to generate topology files for MD simulations, as demonstrated here with selected representative test cases that validate our models and setup procedure (Figure 4). These topology parameters are compatible with the AMBER family of force fields, allowing the simulation of the nanosystems in conjunction with other biologically relevant macromolecules, such as proteins, nucleic acids, lipids, and carbohydrates.

Upcoming features of NanoModeler may include a fragment-based library for the in-site building of the coating thiols, and partial charges estimation. Future versions of NanoModeler will also offer coarse-grained representation of NPs, allowing the automatic assembly and setup of very large systems for MD simulations.[61,91] We intend to patch these features to the current server in future releases. This Webserver is free for use by experimental and computational scientists working on functionalized NPs. We trust that NanoModeler will accelerate new developments in the emerging field of

DOI: 10.1021/acs.jctc.8b01304
J. Chem. Theory Comput. 2019, 15, 2022−2032

computational nanodesign and simulations to engineer functionalized NPs.[92]

WEBSERVER BUILDING

Structure of the Webserver. The NanoModeler Webserver (www.nanomodeler.it) has two main components: the frontend and the backend. The frontend is a single-page application that uses the Angular 6 framework, a TypeScript-based, web-application platform that dynamically rewrites the page for an enhanced user experience. In addition, the graphical interface incorporates the Bootstrap framework, allowing the application to be accessible from various devices (e.g., smartphones, tablets, laptops) without compromising its functionalities. The backend is an aggregation of MicroServices that run in Docker containers. Some containers, like the orchestrator and data persistence layer, are built on top of NodeJS, whereas the code to assemble nanosystems and their topology is written in Python. Below, the assembly of the 3D models and topologies are discussed in detail.

Preparation of Cores and Coatings. Here, we outline NanoModeler's operating steps, as shown in Figure 1A. The assembly of the 3D model of a given NP is based on the initial arrangement of the gold and sulfur atoms, as reported in the literature (Table 1). Thanks to the wealth of atomically detailed data on NPs, NanoModeler implements 16 different cores, ranging from 0.9 to 2.1 nm in diameter. Each core is listed in Table 1, together with its respective size (average diameter) and the name of the coating thiol with which it was first elucidated.

Prior to their implementation, the cores' files were processed with in-house scripts that classify the gold and sulfur atoms on the basis of their relative structural arrangement. In general, the gold−sulfur interface comprises staple-like motifs where each sulfur atom is bound to two gold atoms.[56,90] All staples in the cores are assigned to one of three classes, that is, STR, STC, and STV (Figure 2). The staples are identified and classified on the basis of their Au−S distances and S−Au−S angles. Three types of gold atoms are also differentiated, that is, AUL, AUS, and AU. The AUL and AUS gold atoms are classified on the basis of the position in their respective staple (Figure 2). The remaining gold atoms are classified as AU. All three gold atom types are assigned the same nonbonded parameters; their differentiation is structural only and is necessary for the bonded parameters. All core structures in NanoModeler contain the gold atoms, the sulfur atoms in the staples, and the first carbon of the ligand with which they were originally elucidated (when present, Figure 5A). However, some structures were reported without any bound ligand, that is, without a cis−trans isomerism known a priori. For these cases, vectors were drawn from the centroid of the systems to the sulfur atoms, and a methyl group was positioned away from each sulfur atom at the characteristic thiol carbon−sulfur distance (0.18 nm).[93] After their methylation, the systems were parametrized following the workflow presented below, and minimized using the steepest descent method until the forces were smaller than 250 kJ mol^{-1} nm^{-1} (ca. 500 steps). The hydrogen atoms of the methyl groups then were deleted, and the structure of the core was stored.

To create the functionalized NP, the user must provide the structure of one or two ligands in .mol2 file format. To perform MD simulations, the input files must contain the partial charges of all atoms. In this case, charges may be calculated with the RESP[94,95] approach through the R.E.D. server.[96] The provided ligand structures may have an open valence on the atom that serves as the anchor point to connect the thiol to the core. If so, this will be used to link the ligands to the core. If the ligand contains a capping group (e.g., the hydrogen on the thiol's −S−H group), this must be specified. The atoms and bonds belonging to this group are then removed from the structure to allow linking to the core structure. Special care should be taken here. This is because the charge of the capping group is equally distributed by NanoModeler across the other atoms in the molecule (Figure 5B).

3D Modeling of AuNPs. When building a nanostructure in NanoModeler, the user must specify the core. The server then assigns a morphology by giving each carbon atom from the core a particular label, which defines the ligand to be placed in that position. If only one ligand is uploaded, all labels are the same. If two ligands are uploaded, the labels are assigned depending on the specified morphology type. Currently, three morphologies are supported, "Random", "Janus", and "Stripe". When the morphology is set to "Random" or "Janus", the user may specify the fraction (between 0 and 1) of sites to be labeled with the first ligand. The remaining sites are assigned to the second ligand. When the morphology is set to "Stripe", the azimuthal angle φ is divided into N_s equidistant intervals, where N_s is the number of stripes specified by the user (Figure 5C). The carbon atoms are then labeled in an intercalating fashion depending on the interval into which they fall.

After the morphology is assigned to the core, the structure file of the ligands is read. Regardless of the presence of a capping group in the ligands, the structure may or may not contain the thiol's sulfur atom (namely the S atom), through which it is bound to the metallic core. If S is absent, the user must indicate the carbon atom of the coating molecule (the C atom), which should be covalently bound to S (Figure 5B). In this case, S is placed 0.18 nm from C along the principal axis of the molecule. To calculate the principal axis of a ligand (PC-1), the molecule is translated so that C is the origin of coordinates. PC-1 corresponds to the eigenvector associated with the largest eigenvalue of the covariance matrix. The covariance matrix $\sum$ is constructed with eq 1 from the Cartesian coordinates of all of the atoms:

$$\sum_{ij} = \frac{\sum_{k=1}^{n} (X_i^k - \mu_i)(X_j^k - \mu_j)}{n - 1} \quad (1)$$

where n is the number of atoms, X_i^k is the ith coordinate of the kth atom, and μ_i is the mean of the ith coordinates from all of the atoms. The server then identifies three characteristic points of each ligand for further anchoring. The first point is C. For the other two points, two atoms of each ligand, excluding S and C, are chosen and projected along PC-1. The selection of the latter two points is performed pseudorandomly, so that the results are reproducible given the same input files. The distances d_1 and d_2 between these two points and C are calculated and stored for later use (Figure 5D).

Each carbon atom of the core is then treated sequentially. First, a vector is drawn from the centroid of the core to the carbon atom, in a sequential order. The morphology label on site is read, and the values of d_1 and d_2 of the respective ligand are retrieved. The vector is then scaled to reach a distance d_1 from the carbon atom, and a virtual site is saved at this position. The same procedure is carried out for d_2 (Figure 5E). A quaternion transformation matrix is fitted so that the three

DOI: 10.1021/acs.jctc.8b01304
J. Chem. Theory Comput. 2019, 15, 2022−2032

aforementioned points of the ligand match the carbon atom and the two virtual sites. At this point, the transformation is applied to the ligand to obtain the roto-translated structure. Note that the coordinates of S must be modified to match those of the closest sulfur atom present in the core. The method is thus invariant to the original position of S in the ligands' structure. Because the fitting points are collinear, the roto-translation is arbitrary, and it may result in clashes with the rest of the system. To overcome this, the ligand is rotated along the vector between the centroid of the core and C iteratively. The coordinate is scanned through 100 iterations. For each iteration, the minimum distance between the ligand and the rest of the system is stored. The final orientation results in the largest minimum distance after the entire scanning. The structure of the NP is obtained after repeating this procedure for all ligands (Figure 5F).

MD Simulations. To validate the topologies built with NanoModeler, we simulated three AuNPs, each with different coatings. The three coating thiols were octanethiol (NP1), decanethiol (NP2), and dodecanethiol (NP3). The partial charges of the thiols were calculated with the RESP fitting procedure as implemented in R.E.D. server.[94−96] The initial conformation and the parameter files were generated with NanoModeler.

For the MD runs, a simulation box was built to ensure a minimum distance of 1.0 nm between the AuNP and the box edge. The box was then filled with chloroform molecules, whose parameters are reported elsewhere.[97] To relax the solvent around the particle, a minimization was carried out using the steepest descent method. The system was heated for 500 ps with the V-rescale thermostat (τ_T = 0.1 ps) in the NVT ensemble to 295 K, a temperature chosen to match the experimental conditions used by Terrill et al.[88] We then pressurized the system to 1 bar with a 500 ps-long simulation in the NPT ensemble with the isotropic Parrinello−Rahman barostat (τ_P = 2.0 ps and $\kappa = 10^{-4}$ bar^{-1}).[98] Once the system had reached the intended temperature and pressure, the system was simulated for 200 ns, discarding the first 25 ns as equilibration. All bonds were constrained using the LINCS algorithm,[99] and a time-step of 2 fs was used. Short-range nonbonded interactions were calculated within a radius of 1.2 nm of each atom, whereas long-range electrostatic interactions were considered using the fourth-ordered PME method.[100] The simulations for NP2 were performed in dichloromethane,[97] following the same protocol at 300 K to match the respective experimental conditions.[90] All simulations were conducted with Gromacs-5.1.[101−103]

For the trajectory analysis, we used a mixture of Gromacs tools and in-house scripts. To calculate the average distances between the gold's surface and the carbon atoms, we used eq 2:

$$\langle r_i \rangle = \int_0^{D_{max}} \rho_i(r) r \, dr \tag{2}$$

where $\langle r_i \rangle$ is the mean distance between the gold's surface and the ith carbon of the alkyl chain, D_{max} is one-half of the shortest box vector, and ρ_i is the normalized radial distribution function (RDF) of the ith carbon. The RDF was originally calculated with Gromacs and then normalized to one. To calculate the translational diffusion coefficients, we used the Stokes−Einstein relation (eq 3), following the workflow presented by Piserchia et al.:[90]

$$D_{transl} = \frac{k_B T}{8\pi\eta_{solv} R^3_{hdynamic}} \tag{3}$$

where k_B is Boltzmann constant, T is the temperature, η_{solv} is the experimental viscosity of the solvent, and $R_{hdynamic}$ is the hydrodynamic radius of the NP calculated as the average distance of the most exposed heavy atom from the thiol. The standard deviations shown in Figure 4 were estimated by propagating the uncertainty associated with the probability density function following eq 4:

$$\sigma_{r_i} = [\langle r_i^2 \rangle - \langle r_i \rangle^2]^{1/2} \tag{4}$$

The radius of gyration was calculated with the "gyrate" tool available in Gromacs. All of the aforementioned properties were calculated from snapshots saved every 10 ps.

AUTHOR INFORMATION

Corresponding Author

*E-mail: marco.devivo@iit.it.

ORCID

Marco De Vivo: 0000-0003-4022-5661

Funding

M.D.V. thanks the Italian Association for Cancer Research (AIRC) for financial support (grant no. 18883).

Notes

The authors declare no competing financial interest.

ACKNOWLEDGMENTS

M.D.V. thanks PRACE for supercomputer time. We thank Grace Fox for proofreading and copyediting the manuscript. We also thank all our research collaborators for testing NanoModeler and for their formative feedback during the debugging and developing stages.

REFERENCES

(1) Riccardi, L.; Gabrielli, L.; Sun, X.; De Biasi, F.; Rastrelli, F.; Mancin, F.; De Vivo, M. Nanoparticle-Based Receptors Mimic Protein-Ligand Recognition. *Chem.* **2017**, *3* (1), 92−109.

(2) Diez-Castellnou, M.; Mancin, F.; Scrimin, P. Efficient Phosphodiester Cleaving Nanozymes Resulting from Multivalency and Local Medium Polarity Control. *J. Am. Chem. Soc.* **2014**, *136* (4), 1158−1161.

(3) Manea, F.; Houillon, F. B.; Pasquato, L.; Scrimin, P. Nanozymes: Gold-Nanoparticle-Based Transphosphorylation Catalysts. *Angew. Chem., Int. Ed.* **2004**, *43* (45), 6165−6169.

(4) Pasquato, L.; Pengo, P.; Scrimin, P. Nanozymes: Functional Nanoparticle-Based Catalysts. *Supramol. Chem.* **2005**, *17* (1−2), 163−171.

(5) Makarucha, A. J.; Todorova, N.; Yarovsky, I. Nanomaterials in Biological Environment: A Review of Computer Modelling Studies. *Eur. Biophys. J.* **2011**, *40* (2), 103−115.

(6) Riley, R. S.; Day, E. S. Gold Nanoparticle-Mediated Photothermal Therapy: Applications and Opportunities for Multimodal Cancer Treatment. *Wiley Interdiscip. Rev. Nanomedicine Nanobiotechnology* **2017**, *9* (4), e1449.

(7) Torchi, A.; Simonelli, F.; Ferrando, R.; Rossi, G. Local Enhancement of Lipid Membrane Permeability Induced by Irradiated Gold Nanoparticles. *ACS Nano* **2017**, *11* (12), 12553−12561.

(8) Stern, J. M.; Kibanov Solomonov, V. V.; Sazykina, E.; Schwartz, J. A.; Gad, S. C.; Goodrich, G. P. Initial Evaluation of the Safety of Nanoshell-Directed Photothermal Therapy in the Treatment of Prostate Disease. *Int. J. Toxicol.* **2016**, *35* (1), 38−46.

DOI: 10.1021/acs.jctc.8b01304
J. Chem. Theory Comput. 2019, 15, 2022−2032

(9) Lee, B. K.; Yun, Y. H.; Park, K. Smart Nanoparticles for Drug Delivery: Boundaries and Opportunities. *Chem. Eng. Sci.* **2015**, *125* (2), 158−164.
(10) Yang, Y.; Ren, L.; Wang, H. Strategies in the Design of Gold Nanoparticles for Intracellular Targeting: Opportunities and Challenges. *Ther. Delivery* **2017**, *8* (10), 879−897.
(11) Ding, H. M.; Ma, Y. Q. Theoretical and Computational Investigations of Nanoparticle-Biomembrane Interactions in Cellular Delivery. *Small* **2015**, *11* (9−10), 1055−1071.
(12) Guarise, C.; Pasquato, L.; De Filippis, V.; Scrimin, P. Gold Nanoparticles-Based Protease Assay. *Proc. Natl. Acad. Sci. U. S. A.* **2006**, *103* (11), 3978−3982.
(13) Kinnear, C.; Moore, T. L.; Rodriguez-Lorenzo, L.; Rothen-Rutishauser, B.; Petri-Fink, A. Form Follows Function: Nanoparticle Shape and Its Implications for Nanomedicine. *Chem. Rev.* **2017**, *117* (17), 11476−11521.
(14) Pedone, D.; Moglianetti, M.; De Luca, E.; Bardi, G.; Pompa, P. P. Platinum Nanoparticles in Nanobiomedicine. *Chem. Soc. Rev.* **2017**, *46* (16), 4951−4975.
(15) Sun, X.; Liu, P.; Mancin, F. Sensor Arrays Made by Self-Organized Nanoreceptors for Detection and Discrimination of Carboxylate Drugs. *Analyst* **2018**, *143*, 5754.
(16) Jha, S.; Ramadori, F.; Quarta, S.; Biasiolo, A.; Fabris, E.; Baldan, P.; Guarino, G.; Ruvoletto, M.; Villano, G.; Turato, C.; et al. Binding and Uptake into Human Hepatocellular Carcinoma Cells of Peptide-Functionalized Gold Nanoparticles. *Bioconjugate Chem.* **2017**, *28* (1), 222−229.
(17) Liu, X.; Yu, M.; Kim, H.; Mameli, M.; Stellacci, F. Determination of Monolayer-Protected Gold Nanoparticle Ligand−shell Morphology Using NMR. *Nat. Commun.* **2012**, *3* (1), 1182.
(18) Moglianetti, M.; De Luca, E.; Pedone, D.; Marotta, R.; Catelani, T.; Sartori, B.; Amenitsch, H.; Retta, S. F.; Pompa, P. P. Platinum Nanozymes Recover Cellular ROS Homeostasis in an Oxidative Stress-Mediated Disease Model. *Nanoscale* **2016**, *8* (6), 3739−3752.
(19) De Vivo, M.; Masetti, M.; Bottegoni, G.; Cavalli, A. Role of Molecular Dynamics and Related Methods in Drug Discovery. *J. Med. Chem.* **2016**, *59* (9), 4035−4061.
(20) De Vivo, M.; Cavalli, A. Recent Advances in Dynamic Docking for Drug Discovery. *Wiley Interdiscip. Rev. Comput. Mol. Sci.* **2017**, *7* (6), e1320.
(21) Salorinne, K.; Malola, S.; Wong, O. A.; Rithner, C. D.; Chen, X.; Ackerson, C. J.; Häkkinen, H. Conformation and Dynamics of the Ligand Shell of a Water-Soluble Au_{102} Nanoparticle. *Nat. Commun.* **2016**, *7*, 10401.
(22) Van Lehn, R. C.; Ricci, M.; Silva, P. H. J.; Andreozzi, P.; Reguera, J.; Voïtchovsky, K.; Stellacci, F.; Alexander-Katz, A. Lipid Tail Protrusions Mediate the Insertion of Nanoparticles into Model Cell Membranes. *Nat. Commun.* **2014**, *5* (1), 4482.
(23) Van Lehn, R. C.; Alexander-Katz, A. Pathway for Insertion of Amphiphilic Nanoparticles into Defect-Free Lipid Bilayers from Atomistic Molecular Dynamics Simulations. *Soft Matter* **2015**, *11* (16), 3165−3175.
(24) Van Lehn, R. C.; Alexander-Katz, A. Membrane-Embedded Nanoparticles Induce Lipid Rearrangements Similar to Those Exhibited by Biological Membrane Proteins. *J. Phys. Chem. B* **2014**, *118* (44), 12586−12598.
(25) Patitsa, M.; Karathanou, K.; Kanaki, Z.; Tzioga, L.; Pippa, N.; Demetzos, C.; Verganelakis, D. A.; Cournia, Z.; Klinakis, A. Magnetic Nanoparticles Coated with Polyarabic Acid Demonstrate Enhanced Drug Delivery and Imaging Properties for Cancer Theranostic Applications. *Sci. Rep.* **2017**, *7* (1), 775.
(26) Heikkilä, E.; Martinez-Seara, H.; Gurtovenko, A. A.; Javanainen, M.; Häkkinen, H.; Vattulainen, I.; Akola, J. Cationic Au Nanoparticle Binding with Plasma Membrane-like Lipid Bilayers: Potential Mechanism for Spontaneous Permeation to Cells Revealed by Atomistic Simulations. *J. Phys. Chem. C* **2014**, *118* (20), 11131−11141.
(27) Salassi, S.; Simonelli, F.; Bochicchio, D.; Ferrando, R.; Rossi, G. Au Nanoparticles in Lipid Bilayers: A Comparison between Atomistic and Coarse-Grained Models. *J. Phys. Chem. C* **2017**, *121* (20), 10927−10935.
(28) Van Lehn, R. C.; Alexander-Katz, A. Energy Landscape for the Insertion of Amphiphilic Nanoparticles into Lipid Membranes: A Computational Study. *PLoS One* **2019**, *14* (1), e0209492.
(29) Pederzoli, F.; Tosi, G.; Vandelli, M. A.; Belletti, D.; Forni, F.; Ruozi, B. Protein Corona and Nanoparticles: How Can We Investigate On? *Wiley Interdiscip. Rev. Nanomedicine Nanobiotechnology* **2017**, *9* (6), 1−23.
(30) Ding, F.; Radic, S.; Chen, R.; Chen, P.; Geitner, N. K.; Brown, J. M.; Ke, P. C. Direct Observation of a Single Nanoparticle−ubiquitin Corona Formation. *Nanoscale* **2013**, *5* (19), 9162−9169.
(31) Olenick, L. L.; Troiano, J. M.; Vartanian, A.; Melby, E. S.; Mensch, A. C.; Zhang, L.; Hong, J.; Qiu, T.; Bozich, J.; Lohse, S. Lipid Corona Formation from Nanoparticle Interactions with Bilayers and Membrane-Specific Biological Outcomes. *Chem.* **2018**, *4*, 2709.
(32) Villarreal, O. D.; Rodriguez, R. A.; Yu, L.; Wambo, T. O. Molecular Dynamics Simulations on the Effect of Size and Shape on the Interactions between Negative $Au_{18}(SR)_{14}$, $Au_{102}(SR)_{44}$ and $Au_{144}(SR)_{60}$ Nanoparticles in Physiological Saline. *Colloids Surf., A* **2016**, *503*, 70−78.
(33) Villarreal, O. D.; Chen, L. Y.; Whetten, R. L.; Yacaman, M. J. Ligand-Modulated Interactions between Charged Monolayer-Protected $Au_{144}(SR)_{60}$ Gold Nanoparticles in Physiological Saline. *Phys. Chem. Chem. Phys.* **2015**, *17* (5), 3680−3688.
(34) Chatzigoulas, A.; Karathanou, K.; Dellis, D.; Cournia, Z. NanoCrystal: A Web-Based Crystallographic Tool for the Construction of Nanoparticles Based on Their Crystal Habit. *J. Chem. Inf. Model.* **2018**, *58*, 2380.
(35) Case, D. A.; Betz, R. M.; Cerutti, D. S.; Cheatham, T. E., III; Darden, T. A.; Duke, R. E.; Giese, T. J.; Gohlke, H.; Goetz, A. W.; Homeyer, N.; et al. *AMBER 2016*; University of California: San Francisco, CA, 2016.
(36) Wang, J.; Wang, W.; Kollman, P. A.; Case, D. A. Automatic Atom Type and Bond Type Perception in Molecular Mechanical Calculations. *J. Mol. Graphics Modell.* **2006**, *25* (2), 247−260.
(37) Vanommeslaeghe, K.; Raman, E. P.; MacKerell, A. D. J. Automation of the CHARMM General Force Field (CGenFF) II: Assignment of Bonded Parameters and Partial Atomic Charges. *J. Chem. Inf. Model.* **2012**, *52* (12), 3155−3168.
(38) Anandakrishnan, R.; Aguilar, B.; Onufriev, A. V. H++ 3.0: Automating PK Prediction and the Preparation of Biomolecular Structures for Atomistic Molecular Modeling and Simulations. *Nucleic Acids Res.* **2012**, *40* (Web Server), W537−W541.
(39) van Dijk, M.; Bonvin, A. M. J. J. 3D-DART: A DNA Structure Modelling Server. *Nucleic Acids Res.* **2009**, *37* (Web Server), W235−W239.
(40) Colasanti, A. V.; Lu, X.-J.; Olson, W. K. Analyzing and Building Nucleic Acid Structures with 3DNA. *J. Visualized Exp.* **2013**, *74*, e4401.
(41) Dodda, L. S.; Cabeza de Vaca, I.; Tirado-Rives, J.; Jorgensen, W. L. LigParGen Web Server: An Automatic OPLS-AA Parameter Generator for Organic Ligands. *Nucleic Acids Res.* **2017**, *45* (Web Server), W331−W336.
(42) Jo, S.; Kim, T.; Iyer, V. G.; Im, W. CHARMM-GUI: A Web-Based Graphical User Interface for CHARMM. *J. Comput. Chem.* **2008**, *29* (11), 1859−1865.
(43) Ghahremanpour, M. M.; Arab, S. S.; Aghazadeh, S. B.; Zhang, J.; van der Spoel; MemBuilder, D. A Web-Based Graphical Interface to Build Heterogeneously Mixed Membrane Bilayers for the GROMACS Biomolecular Simulation Program. *Bioinformatics* **2014**, *30* (3), 439−441.
(44) Wassenaar, T. A.; Ingólfsson, H. I.; Böckmann, R. A.; Tieleman, D. P.; Marrink, S. J. Computational Lipidomics with Insane: A Versatile Tool for Generating Custom Membranes for Molecular Simulations. *J. Chem. Theory Comput.* **2015**, *11* (5), 2144−2155.

DOI: 10.1021/acs.jctc.8b01304
J. Chem. Theory Comput. 2019, 15, 2022−2032

(45) Sakthivel, N. A.; Theivendran, S.; Ganeshraj, V.; Oliver, A. G.; Dass, A. Crystal Structure of Faradaurate-279: $Au_{279}(SPh - TBu)_{84}$ Plasmonic Nanocrystal Molecules. *J. Am. Chem. Soc.* **2017**, *139* (43), 15450−15459.
(46) Bahena, D.; Bhattarai, N.; Santiago, U.; Tlahuice, A.; Ponce, A.; Bach, S. B. H.; Yoon, B.; Whetten, R. L.; Landman, U.; Jose-Yacaman, M. STEM Electron Diffraction and High-Resolution Images Used in the Determination of the Crystal Structure of the $Au_{144}(SR)_{60}$ Cluster. *J. Phys. Chem. Lett.* **2013**, *4* (6), 975−981.
(47) Jensen, K. M. Ø.; Juhas, P.; Tofanelli, M. A.; Heinecke, C. L.; Vaughan, G.; Ackerson, C. J.; Billinge, S. J. L. Polymorphism in Magic-Sized $Au_{144}(SR)_{60}$ Clusters. *Nat. Commun.* **2016**, *7*, 11859.
(48) Malola, S.; Lehtovaara, L.; Enkovaara, J.; Häkkinen, H. Birth of the Localized Surface Plasmon Resonance in Monolayer-Protected Gold Nanoclusters. *ACS Nano* **2013**, *7* (11), 10263−10270.
(49) Marsella, A.; Valentini, P.; Tarantino, P.; Congedo, M.; Pompa, P. P. In *A Gold Nanoparticles-Based Colorimetric Test to Detect Single Nucleotide Polymorphisms for Improvement of Personalized Therapy of Psoriasis*; Popp, J., Tuchin, V. V., Matthews, D. L., Pavone, F. S., Eds.; SPIE, 2016; Vol. *9887*, p 98870P.
(50) Aldewachi, H.; Chalati, T.; Woodroofe, M. N.; Bricklebank, N.; Sharrack, B.; Gardiner, P. Gold Nanoparticle-Based Colorimetric Biosensors. *Nanoscale* **2018**, *10* (1), 18−33.
(51) Cole, L. E.; Ross, R. D.; Tilley, J. M.; Vargo-Gogola, T.; Roeder, R. K. Gold Nanoparticles as Contrast Agents in X-Ray Imaging and Computed Tomography. *Nanomedicine* **2015**, *10* (2), 321−341.
(52) Popovtzer, R.; Agrawal, A.; Kotov, N. A.; Popovtzer, A.; Balter, J.; Carey, T. E.; Kopelman, R. Targeted Gold Nanoparticles Enable Molecular CT Imaging of Cancer. *Nano Lett.* **2008**, *8* (12), 4593−4596.
(53) Blanco, E.; Shen, H.; Ferrari, M. Principles of Nanoparticle Design for Overcoming Biological Barriers to Drug Delivery. *Nat. Biotechnol.* **2015**, *33* (9), 941−951.
(54) Lucarini, M.; Pasquato, L. ESR Spectroscopy as a Tool to Investigate the Properties of Self-Assembled Monolayers Protecting Gold Nanoparticles. *Nanoscale* **2010**, *2* (5), 668−676.
(55) Bürgi, T. Properties of the Gold−sulphur Interface: From Self-Assembled Monolayers to Clusters. *Nanoscale* **2015**, *7* (38), 15553−15567.
(56) Häkkinen, H. The Gold−sulfur Interface at the Nanoscale. *Nat. Chem.* **2012**, *4* (6), 443−455.
(57) Dolamic, I.; Varnholt, B.; Bürgi, T. Far-Infrared Spectra of Well-Defined Thiolate-Protected Gold Clusters. *Phys. Chem. Chem. Phys.* **2013**, *15* (45), 19561−19565.
(58) Knoppe, S.; Bürgi, T. Chirality in Thiolate-Protected Gold Clusters. *Acc. Chem. Res.* **2014**, *47* (4), 1318−1326.
(59) Dolamic, I.; Varnholt, B.; Bürgi, T. Chirality Transfer from Gold Nanocluster to Adsorbate Evidenced by Vibrational Circular Dichroism. *Nat. Commun.* **2015**, *6*, 7117.
(60) Luo, Z.; Zhao, Y.; Darwish, T.; Wang, Y.; Hou, J.; Stellacci, F. Mass Spectrometry and Monte Carlo Method Mapping of Nanoparticle Ligand Shell Morphology. *Nat. Commun.* **2018**, *9* (1), 4478.
(61) Gkeka, P.; Sarkisov, L.; Angelikopoulos, P. Homogeneous Hydrophobic-Hydrophilic Surface Patterns Enhance Permeation of Nanoparticles through Lipid Membranes. *J. Phys. Chem. Lett.* **2013**, *4* (11), 1907−1912.
(62) Pengo, P.; Sologan, M.; Pasquato, L.; Guida, F.; Pacor, S.; Tossi, A.; Stellacci, F.; Marson, D.; Boccardo, S.; Pricl, S.; et al. Gold Nanoparticles with Patterned Surface Monolayers for Nanomedicine: Current Perspectives. *Eur. Biophys. J.* **2017**, *46*, 749−771.
(63) Lee, M. W.; Han, M.; Bossa, G. V.; Snell, C.; Song, Z.; Tang, H.; Yin, L.; Cheng, J.; May, S.; Luijten, E.; et al. Interactions between Membranes and "Metaphilic" Polypeptide Architectures with Diverse Side-Chain Populations. *ACS Nano* **2017**, *11* (3), 2858−2871.
(64) Walther, A.; Müller, A. H. E. Janus Particles: Synthesis, Self-Assembly, Physical Properties, and Applications. *Chem. Rev.* **2013**, *113* (7), 5194−5261.
(65) Huang, J.; Kim, F.; Tao, A. R.; Connor, S.; Yang, P. Spontaneous Formation of Nanoparticle Stripe Patterns through Dewetting. *Nat. Mater.* **2005**, *4* (12), 896−900.
(66) Stirling, J.; Lekkas, I.; Sweetman, A.; Djuranovic, P.; Guo, Q.; Pauw, B.; Granwehr, J.; Lévy, R.; Moriarty, P. Critical Assessment of the Evidence for Striped Nanoparticles. *PLoS One* **2014**, *9* (11), e108482.
(67) Ong, Q. K.; Stellacci, F. Response to "Critical Assessment of the Evidence for Striped Nanoparticles. *PLoS One* **2015**, *10* (11), e0135594.
(68) Lee, K.; Zhang, L.; Yi, Y.; Wang, X.; Yu, Y. Rupture of Lipid Membranes Induced by Amphiphilic Janus Nanoparticles. *ACS Nano* **2018**, *12* (4), 3646−3657.
(69) Velachi, V.; Bhandary, D.; Singh, J. K.; Cordeiro, M. N. D. S. Structure of Mixed Self-Assembled Monolayers on Gold Nanoparticles at Three Different Arrangements. *J. Phys. Chem. C* **2015**, *119* (6), 3199−3209.
(70) Verma, A.; Stellacci, F. Effect of Surface Properties on Nanoparticle-Cell Interactions. *Small* **2010**, *6* (1), 12−21.
(71) Gkeka, P.; Angelikopoulos, P. The Role of Patterned Hydrophilic Domains in Nanoparticle-Membrane Interactions. *Curr. Nanosci.* **2011**, *7* (5), 690−698.
(72) Pohjolainen, E.; Chen, X.; Malola, S.; Groenhof, G.; Häkkinen, H. A Unified AMBER-Compatible Molecular Mechanics Force Field for Thiolate-Protected Gold Nanoclusters. *J. Chem. Theory Comput.* **2016**, *12* (3), 1342−1350.
(73) Heinz, H.; Vaia, R. A.; Farmer, B. L.; Naik, R. R. Accurate Simulation of Surfaces and Interfaces of Face-Centered Cubic Metals Using 12−6 and 9−6 Lennard-Jones Potentials. *J. Phys. Chem. C* **2008**, *112* (44), 17281−17290.
(74) Heikkilä, E.; Gurtovenko, A. A.; Martinez-Seara, H.; Häkkinen, H.; Vattulainen, I.; Akola, J. Atomistic Simulations of Functional $Au_{144}(SR)_{60}$ Gold Nanoparticles in Aqueous Environment. *J. Phys. Chem. C* **2012**, *116* (17), 9805−9815.
(75) Wang, J.; Wolf, R. M.; Caldwell, J. W.; Kollman, P. A.; Case, D. A. Development and Testing of a General Amber Force Field. *J. Comput. Chem.* **2004**, *25* (9), 1157−1174.
(76) Sousa da Silva, A. W.; Vranken, W. F. ACPYPE - AnteChamber PYthon Parser InterfacE. *BMC Res. Notes* **2012**, *5* (1), 367.
(77) Maier, J. A.; Martinez, C.; Kasavajhala, K.; Wickstrom, L.; Hauser, K. E.; Simmerling, C. FF14SB: Improving the Accuracy of Protein Side Chain and Backbone Parameters from FF99SB. *J. Chem. Theory Comput.* **2015**, *11* (8), 3696−3713.
(78) Lindorff-Larsen, K.; Piana, S.; Palmo, K.; Maragakis, P.; Klepeis, J. L.; Dror, R. O.; Shaw, D. E. Improved Side-Chain Torsion Potentials for the Amber FF99SB Protein Force Field. *Proteins: Struct., Funct., Genet.* **2010**, *78* (8), 1950−1958.
(79) Ivani, I.; Dans, P. D.; Noy, A.; Pérez, A.; Faustino, I.; Hospital, A.; Walther, J.; Andrio, P.; Goñi, R.; Balaceanu, A.; et al. Parmbsc1: A Refined Force Field for DNA Simulations. *Nat. Methods* **2016**, *13* (1), 55−58.
(80) Pérez, A.; Marchán, I.; Svozil, D.; Sponer, J.; Cheatham, T. E.; Laughton, C. A.; Orozco, M. Refinement of the AMBER Force Field for Nucleic Acids: Improving the Description of Alpha/Gamma Conformers. *Biophys. J.* **2007**, *92* (11), 3817−3829.
(81) Genna, V.; Vidossich, P.; Ippoliti, E.; Carloni, P.; De Vivo, M. A Self-Activated Mechanism for Nucleic Acid Polymerization Catalyzed by DNA/RNA Polymerases. *J. Am. Chem. Soc.* **2016**, *138* (44), 14592−14598.
(82) Genna, V.; Carloni, P.; De Vivo, M. A Strategically Located Arg/Lys Residue Promotes Correct Base Paring During Nucleic Acid Biosynthesis in Polymerases. *J. Am. Chem. Soc.* **2018**, *140* (9), 3312−3321.
(83) Genna, V.; Gaspari, R.; Dal Peraro, M.; De Vivo, M. Cooperative Motion of a Key Positively Charged Residue and Metal Ions for DNA Replication Catalyzed by Human DNA Polymerase-η. *Nucleic Acids Res.* **2016**, *44* (6), 2827−2836.

DOI: 10.1021/acs.jctc.8b01304
J. Chem. Theory Comput. 2019, 15, 2022−2032

(84) Dickson, C. J.; Madej, B. D.; Skjevik, Å. A.; Betz, R. M.; Teigen, K.; Gould, I. R.; Walker, R. C. Lipid14: The Amber Lipid Force Field. *J. Chem. Theory Comput.* **2014**, *10* (2), 865−879.
(85) Skjevik, Å. A.; Madej, B. D.; Walker, R. C.; Teigen, K. LIPID11: A Modular Framework for Lipid Simulations Using Amber. *J. Phys. Chem. B* **2012**, *116* (36), 11124−11136.
(86) Riccardi, L.; Arencibia, J. M.; Bono, L.; Armirotti, A.; Girotto, S.; De Vivo, M. Lid Domain Plasticity and Lipid Flexibility Modulate Enzyme Specificity in Human Monoacylglycerol Lipase. *Biochim. Biophys. Acta, Mol. Cell Biol. Lipids* **2017**, *1862* (5), 441−451.
(87) Kirschner, K. N.; Yongye, A. B.; Tschampel, S. M.; González-Outeiriño, J.; Daniels, C. R.; Foley, B. L.; Woods, R. J. GLYCAM06: A Generalizable Biomolecular Force Field. Carbohydrates. *J. Comput. Chem.* **2008**, *29* (4), 622−655.
(88) Terrill, R. H.; Postlethwaite, T. A.; Chen, C. H. H.; Poon, C. D. D.; Terzis, A.; Chen, A.; Hutchison, J. E.; Clark, M. R.; Wignall, G.; Londono, J. D.; et al. Monolayers in Three Dimensions: NMR, SAXS, Thermal, and Electron Hopping Studies of Alkanethiol Stabilized Gold Clusters. *J. Am. Chem. Soc.* **1995**, *117* (50), 12537−12548.
(89) Lin, J.; Zhang, H.; Chen, Z.; Zheng, Y. Penetration of Lipid Membranes by Gold Nanoparticles: Insights into Cellular Uptake, Cytotoxicity, and Their Relationship. *ACS Nano* **2010**, *4* (9), 5421−5429.
(90) Piserchia, A.; Zerbetto, M.; Salvia, M.-V.; Salassa, G.; Gabrielli, L.; Mancin, F.; Rastrelli, F.; Frezzato, D. Conformational Mobility in Monolayer-Protected Nanoparticles: From Torsional Free Energy Profiles to NMR Relaxation. *J. Phys. Chem. C* **2015**, *119* (34), 20100−20110.
(91) Simonelli, F.; Bochicchio, D.; Ferrando, R.; Rossi, G. Monolayer-Protected Anionic Au Nanoparticles Walk into Lipid Membranes Step by Step. *J. Phys. Chem. Lett.* **2015**, *6* (16), 3175−3179.
(92) Riccardi, L.; Genna, V.; De Vivo, M. Metal−ligand Interactions in Drug Design. *Nat. Rev. Chem.* **2018**, *2* (7), 100−112.
(93) Trinajstić, N. Calculation of Carbon-Sulphur Bond Lengths. *Tetrahedron Lett.* **1968**, *9* (12), 1529−1532.
(94) Cornell, W. D.; Cieplak, P.; Bayly, C. I.; Kollmann, P. A. Application of RESP Charges to Calculate Conformational Energies, Hydrogen Bond Energies, and Free Energies of Solvation. *J. Am. Chem. Soc.* **1993**, *115* (21), 9620−9631.
(95) Wang, J.; Cieplak, P.; Kollman, P. A. How Well Does a Restrained Electrostatic Potential (RESP) Model Perform in Calculating Conformational Energies of Organic and Biological Molecules? *J. Comput. Chem.* **2000**, *21* (12), 1049−1074.
(96) Vanquelef, E.; Simon, S.; Marquant, G.; Garcia, E.; Klimerak, G.; Delepine, J. C.; Cieplak, P.; Dupradeau, F. Y. R.E.D. Server: A Web Service for Deriving RESP and ESP Charges and Building Force Field Libraries for New Molecules and Molecular Fragments. *Nucleic Acids Res.* **2011**, *39* (Web Server), W511−W517.
(97) Caleman, C.; van Maaren, P. J.; Hong, M.; Hub, J. S.; Costa, L. T.; van der Spoel, D. Force Field Benchmark of Organic Liquids: Density, Enthalpy of Vaporization, Heat Capacities, Surface Tension, Isothermal Compressibility, Volumetric Expansion Coefficient, and Dielectric Constant. *J. Chem. Theory Comput.* **2012**, *8* (1), 61−74.
(98) Parrinello, M.; Rahman, A. Polymorphic Transitions in Single Crystals: A New Molecular Dynamics Method. *J. Appl. Phys.* **1981**, *52* (12), 7182−7190.
(99) Hess, B.; Bekker, H.; Berendsen, H. J. C.; Fraaije, J. G. E. M. LINCS: A Linear Constraint Solver for Molecular Simulations. *J. Comput. Chem.* **1997**, *18* (12), 1463−1472.
(100) Darden, T.; York, D.; Pedersen, L. Particle Mesh Ewald: An N Log(N) Method for Ewald Sums in Large Systems. *J. Chem. Phys.* **1993**, *98* (12), 10089−10092.
(101) Hess, B.; Kutzner, C.; van der Spoel, D.; Lindahl, E. GROMACS 4: Algorithms for Highly Efficient, Load-Balanced, and Scalable Molecular Simulation. *J. Chem. Theory Comput.* **2008**, *4* (3), 435−447.
(102) van der Spoel, D.; Lindahl, E.; Hess, B.; Groenhof, G.; Mark, A. E.; Berendsen, H. J. C. GROMACS: Fast, Flexible, and Free. *J. Comput. Chem.* **2005**, *26* (16), 1701−1718.
(103) Abraham, M. J.; Murtola, T.; Schulz, R.; Pall, S.; Smith, J. C.; Hess, B.; Lindah, E. Gromacs: High Performance Molecular Simulations through Multi-Level Parallelism from Laptops to Supercomputers. *SoftwareX* **2015**, *1−2*, 19−25.
(104) Zhu, M.; Aikens, C. M.; Hollander, F. J.; Schatz, G. C.; Jin, R. Correlating the Crystal Structure of A Thiol-Protected Au_{25} Cluster and Optical Properties. *J. Am. Chem. Soc.* **2008**, *130* (18), 5883−5885.
(105) Das, A.; Liu, C.; Zeng, C.; Li, G.; Li, T.; Rosi, N. L.; Jin, R. Cyclopentanethiolato-Protected $Au_{36}(SC_5H_9)_{24}$ Nanocluster: Crystal Structure and Implications for the Steric and Electronic Effects of Ligand. *J. Phys. Chem. A* **2014**, *118* (37), 8264−8269.
(106) Qian, H.; Eckenhoff, W. T.; Zhu, Y.; Pintauer, T.; Jin, R. Total Structure Determination of Thiolate-Protected Au_{38} Nanoparticles. *J. Am. Chem. Soc.* **2010**, *132* (24), 8280−8281.
(107) Pei, Y.; Lin, S.; Su, J.; Liu, C. Structure Prediction of $Au_{44}(SR)_{28}$: A Chiral Superatom Cluster. *J. Am. Chem. Soc.* **2013**, *135* (51), 19060−19063.
(108) Xu, W. W.; Gao, Y.; Zeng, X. C. Unraveling Structures of Protection Ligands on Gold Nanoparticle Au68(SH)32. *Sci. Adv.* **2015**, *1* (3), e1400211.
(109) Xu, W. W.; Gao, Y. Unraveling the Atomic Structures of the $Au_{68}(SR)_{34}$ Nanoparticles. *J. Phys. Chem. C* **2015**, *119* (25), 14224−14229.
(110) Jadzinsky, P. D.; Calero, G.; Ackerson, C. J.; Bushnell, D. A.; Kornberg, R. D. Structure of a Thiol Monolayer-Protected Gold Nanoparticle at 1.1 A Resolution. *Science* **2007**, *318* (5849), 430−433.
(111) Zeng, C.; Chen, Y.; Kirschbaum, K.; Appavoo, K.; Sfeir, M. Y.; Jin, R. Structural Patterns at All Scales in a Nonmetallic Chiral $Au_{133}(SR)_{52}$ Nanoparticle. *Sci. Adv.* **2015**, *1* (2), e1500045.
(112) Lopez-Acevedo, O.; Akola, J.; Whetten, R. L.; Grönbeck, H.; Häkkinen, H. Structure and Bonding in the Ubiquitous Icosahedral Metallic Gold Cluster $Au_{144}(SR)_{60}$. *J. Phys. Chem. C* **2009**, *113* (13), 5035−5038.

DOI: 10.1021/acs.jctc.8b01304
J. Chem. Theory Comput. 2019, 15, 2022−2032